Strength Evolution in Debinding and Sintering

Randall M. German
Brush Chair Professor in Materials
Center for Innovative Sintered Products
P/M Lab, 147 Research West
Pennsylvania State University
University Park, PA 16802-6809 USA

Abstract

During debinding the pore structure starts as a fully saturated body. As the polymer softens, the component undergoes a strength loss. However, sintering generates strength in the powder sufficient to make the product competitive with other traditional processes such as castings and forgings. Subsieve powders with high inherent sinterability provide one means to attain densification, but at a substantial cost penalty when compared with readily available coarse compaction grade powders. Unfortunately, for large powders the sintering stress that causes densification is small and often insufficient to overcome the inherent compact strength that resists rapid densification. In such cases, only slow diffusion-controlled densification occurs. The current analysis identifies an option for sintering densification of large particles based on a comparison of the sintering stress and component strength during heating. Rapid densification occurs when the *in situ* strength is reduced to levels comparable to the sintering stress. On this basis, alloy systems are identified for full density sintering using thermal softening concepts.

Introduction

Sintering involves heating packed particles to a temperature where atomic motion leads to growth of weld bonds between contacting particles. With higher temperatures or longer holds at the peak temperature, more cumulative atomic motion occurs, leading to improved interparticle bonding. For small powders, densification usually accompanies particle bonding. However, high temperatures, long times, and small particle sizes are not always economically viable for production sintering operations. Thus, most powder metallurgy sintering is performed under conditions where little densification occurs [1].

An early model for sintering by atomic diffusion was formulated by Kuczynski [2]. A teaching from this and many subsequent models is that long times are required to induce diffusion-controlled densification of large particles. As an example, 127 μm copper spheres change from 60% to 67% density after 300 h at 1020°C; but 9 μm copper spheres go from 70% to 94% density after 1 h at 900°C [3]. The 14-fold particle size reduction gives a thousand-fold faster average sintering rate in spite of the lower temperature. However, diffusion-controlled sintering cannot explain rapid shrinkage often observed during heating. Schatt [4] demonstrated plastic flow occurs during intense periods of rapid shrinkage at the higher temperatures. Dislocation flow decayed during isothermal conditions, giving long-term control to diffusion. Early investigations confirmed plastic flow, especially during heating, even in ceramics [5-21].

A good example of the particle size effect down to the nanoscale was given by Andrievski [22]. These data illustrate the interplay between particle size and temperature during constant heating rate sintering. Here, the 0.05 μm powder undergoes significant densification at a lower temperature when compared with the 5 μm powder, while the 50 μm powder is more resistant to sintering densification. Such strong sensitivity to particle size can be explained by the balance between the sintering stress, generated by the capillary forces associated with small particles and the compact strength due to combined parent material strength and neck growth between particles. Rapid sintering densification occurs when the sintering stress exceeds the instantaneous component strength.

Thus, one reason for difficulty in the sinter densification of large particles traces to the compact strength evolution during heating [23,24]. Engineering materials generally exhibit lower strengths at elevated temperatures. For example, pure nickel loses 35% of its room temperature strength by 600°C. On the other hand, powder compacts are weak at room temperature and strengthen during heating as interparticle bond grow by diffusion processes. Surface transport is favored at low temperatures, resulting in bond growth and strengthening without densification. Early in heating sinter bond growth by surface diffusion adds strength faster than the parent material loses strength due to thermal softening. Consequently, the powder compact strengthens faster than the parent material is weakening. Sinter strengthening goes on for most of the heating cycle [23,24]. It is the increasing strength due to neck growth compared with the sintering stress that delays densification to temperatures where thermal softening lowers the compact strength to the same level as the sintering stress. Consequently, densification by diffusion events require long times. Alternatively, high temperatures, smaller particles, liquid phases, or applied stresses provide means to accelerate densification by manipulation of the relative component strength with respect to the sintering stress. Particle size is important because of its impact on the sintering stress. This paper considers the balance between component strength evolution in sintering and the sintering stress. Such a balance is used to explain periods of rapid sintering densification during heating.

Sintering Rates

Sintering starts by growing bonds between contacting particles without densification. Diffusion controlled sintering depends on atomic *mobility* and the microstructure *stress* as determined by an inverse function of the particle, grain, or pore size:

$$\textit{sintering rate} = \textit{mobility} \cdot \textit{stress} \qquad \textbf{(1)}$$

Since the 1940's, many investigators have modeled sintering using various diffusion concepts [3]. Olevsky [25] contrasted 36 different models, showing that most follow the character established by Mackenzie and Shuttleworth [26] and Coble [27]. Smaller powders, smaller grains, and smaller pores have more interfacial energy and induce faster sintering at any given temperature. With respect to diffusion-controlled sintering shrinkage, most of the models can be collected into a generic shrinkage strain rate form as follows:

$$\frac{1}{L_O}\,\frac{dL}{dt} = -\,\frac{A}{\eta\ G^m}\,f(V_S)\ \Sigma^n \qquad \textbf{(2)}$$

where L_O is the original length, L is the instantaneous length, A is a combination of material and geometric constants, t is the time, η is the viscosity, G is the grain size (or other controlling microstructure feature), the grain size exponent *m* is typically 3, and the stress exponent *n* is often near 1. The density amplification function $f(V_S)$ relates the actual (local) stress to the bulk (or applied) stress through various functions of the fractional solid density V_S. The stress function can include several factors that enhance or retard densification, including the capillary stress at the particle contacts, applied stresses, gravity, trapped gas, or rigid inclusions. These ideas are similar to creep concepts [28-31].

Usually sintering shrinkage is traced to atomic diffusion, leading to the concept of an effective viscosity [30,32]. Mackenzie and Shuttleworth [26] estimated the effective viscosity of copper during sintering at 850°C as ranging from $2\ 10^8$ and $3\ 10^{11}$ Pa s. Such a high value has been verified by other experiments; for example, Schatt [4] found a value of $2.3\ 10^9$ Pa s for copper sintering at 800°C, Hsueh, *et al.* [32] suggest a viscosity of 10^{13} Pa s for 65% dense alumina at 1275°C, Cai *et al.* [33] gave 10^{11} Pa s for alumina-yttria at 1000°C, and Lal [34] measured a viscosity of 10^9 Pa s for 68% dense bronze sintering at 800°C.

Sintering theory is most accurate for isothermal, low strain rate events where diffusion control is well established. The problem exists in explaining rapid densification during heating [4]. A dynamic balance is proposed between sintering strengthening (neck growth and densification), thermal softening, and the sintering stress (inversely dependent on the microstructure scale). Densification occurs to sustain a balance between the evolving sintering stress (changing with microstructure coarsening) and component strength. This rapid densification is in addition to slower simultaneous diffusion-controlled precesses. Once isothermal conditions are attained, densification further strengthens the compact without further thermal softening, causing a shift to slower diffusion events. However, rapid densification is not observed if the sintering stress remains far below the *in situ* strength, a problem with large particles and low sintering temperatures.

As evidence of strength-controlled sintering densification, note that both densification and distortion exhibit a threshold strength [26,35-37]. For example, in liquid phase sintering, gravity induces microstructure connectivity that produces a higher component strength that provides less distortion than observed in equivalent microgravity sintering [38]. Three-dimensional coordination number measurements confirm the difference in connectivity associated with gravity conditions [39,40]. Further, calculations based on the distortion profile provide an estimate of the *in situ* threshold stress [41], giving values from 0.2 to 25 kPa [34,42]. Accordingly, sintering compacts exhibit a threshold stress (height) that must not be exceeded to prevent distortion during sintering.

Sintering Stress

The sintering rate depends on the sintering stress which consists of several contributions. In the absence of applied pressure, a measure of the stress acting on the microstructure can be derived from the Laplace equation. This local sintering stress $_L$, defined as the surface energy times the surface curvature (inverse of the microstructure size), is given as,

$$\sigma_L = \gamma\ g \left[\frac{1}{R_1} + \frac{1}{R_2}\right] \quad \textbf{(3)}$$

where is the interfacial energy, *g* is a geometric constant, and R_1 and R_2 are the curvature radii at the surface. For a sphere, the two radii are the same and *g* equals 1. Various approximate solutions are available for the sintering geometry based on characteristic curvatures [43-50] with a dominant effect from the particle size, giving a compressive force distributed over the sintering bond area that depends on the sintering situation:

initial stage solid-state sintering with shrinkage as interparticle bonds grow

$$\sigma_L = \gamma_{SV}\left[-\frac{2}{X} + \frac{4(D - X)}{X^2}\right] \qquad \textbf{(4)}$$

initial stage liquid-phase sintering with pendular liquid interparticle bonds

$$\sigma_L = -\frac{5.2\ \gamma_{LV}\cos(\theta)}{D\,\dfrac{\Delta L}{L_o}} \qquad \textbf{(5)}$$

late stage sintering with small grains and rounded pores

$$\sigma_L = -\frac{2\gamma_{SS}}{G} + \frac{2\gamma_{SV}}{r} \qquad \textbf{(6)}$$

late stage sintering with small grains and faceted pores

$$\sigma_L = \frac{\gamma_{SV}}{d_P}\left(N_P^{1/2}\cos(\frac{\phi}{2}) - (N_P - 4)^{1/2}\cos(\frac{\phi}{2}) + 2\sin(\frac{\phi}{2})\right) \qquad \textbf{(7)}$$

final stage sintering with small spherical pores inside the grains

$$\sigma_L = \frac{4\ \gamma_{SV}}{d_P} \qquad \textbf{(8)}$$

where X is the interparticle bond diameter, D is the particle diameter, G is the grain size, L/L_o is the fractional shrinkage, r is the pore surface curvature, is the liquid wetting angle, N_P is the number of pores per grain, is the dihedral angle, and d_P is the pore diameter. The subscripts on surface energy denote solid-vapor (*SV*), solid-solid (*SS*) (grain boundary), and (*LV*) liquid-vapor energies. In late stage sintering, high grain boundary energies and low dihedral angles inhibit densification, corresponding to negative curvatures for r in Eq. 6.

Thus, sintering systems have an inherent local sintering stress that decreases with larger particles or larger pores. However, note the neck stress is nonuniform. Ogbuji [47] performed finite element analysis of the initial stage sintering stress. Using a surface energy of 2 J/m^2, after 2% shrinkage for a 0.4 m powder the calculated peak surface stress was near 1300 MPa, with an average neck stress of 193 MPa. This is near the 144 MPa stress calculated from Eq. 4. Such locally high stresses are responsible for rapid sintering densification during heating [4]. Accordingly, rapid sintering densification can be understood via analysis of the local sintering stress as compared with the temperature dependent *in situ* component threshold strength $_T$, effectively employing a Bingham response model. At low temperatures the threshold strength is high and the compact resists densification. Alternatively, at higher temperatures, thermal softening lowers the threshold strength, allowing densification in response to the sintering stress.

Besides the sintering stress associated with curved surfaces, other factors affect the sintering response and should be included in determining the net sintering stress and densification rate, including external applied stress [51], microstructure coarsening, and retarding effects from inclusions [32] or trapped gases [52]. High applied pressures effectively overwhelm the inherent sintering stress. Consequently, many compositions that normally resist sintering can be densified by the application of an external pressure. Data from various trials show progressive increase in density with applied pressure [53], with nearly a linear pressure effect on density.

The sintering stress calculated using Eqs. 4-8 represents the local stress at the interparticle bond. On the other hand, a bulk stress calculation distributes that same force over the entire compact cross-section. The bulk stress associated with sintering depends on the local sintering stress, number of contacts per particle, and effective area over which the stress is distributed. Conversion to a bulk stress is needed for comparison with experimental strength tests. As a calculation cell, consider a spherical particle of diameter D with N_C connecting bonds to neighboring particles. This is the coordination number where on average half of the contacts are above the sphere center. For sintering spheres the coordination number relates to the solid volume fraction V_S (fractional density) as follows [3]:

$$N_C = 14 - 10.4\ (1 - V_S)^{0.38} \tag{9}$$

Unless compressed to provide mechanical interlocking, the initial contacts are points and only weak similar forces give strength. Sintering grows bonds between the grains, measured by the contact diameter X, providing strength during sintering [54] and in semisolid systems [55,56]. Assume the bonds are randomly oriented with respect to the test axis. Then the bulk sintering strength $_B$ depends on the solid volumetric fractional density V_S, packing coordination N_C, neck size to particle size ratio X/D, and sintering stress as follows:

$$\sigma_B = \Sigma\ V_S\ \frac{N_C}{\pi} \left(\frac{X}{D}\right)^2 \tag{10}$$

The average neck size to particle size ratio X/D is 0.474 to 0.512 if a typical polyhedron grain shape is assumed (N_C = 14 or 12) at full density (V_S= 1), which is near the average experimental value of 0.53 measured by Fischmeister, *et al.* [57]; the upper limit is assumed as 0.5.

Several empirical models for the sintering stress are reviewed by Du and Cocks [58] and Olevsky [25]. Most are combinations of the capillary stress models (Eqs. 4-8) and stress redistribution estimates, spline fit over the range of densities typically encountered in sintering. All of the models show the typical stress is on the order of 1 MPa. But the models differ by about a factor of 3, depending on the assumptions.

A demonstration of the validity of Eq. 10 is in the data from Gregg and Rhines [43]. They stressed copper powder compacts to stop shrinkage during sintering using 12, 30, and 48 m particles and temperatures near 1000°C. A halt to sintering shrinkage (termed the zero creep stress) corresponds to a net stress of zero (= $_L$ - $_T$ = 0). Analysis of their data shows the expected behavior using a threshold stress $_T$ = 0.57 MPa. To perform these calculations the threshold strength $_T$ was fixed and the bulk sintering strength $_B$ was calculated from Eq. 10, with the sintered neck size calculated from the sintered fractional density V_S and initial fractional density V_{So} as follows:

$$\left(\frac{X}{D}\right)^2 = 4\left[1 - \left(\frac{V_{So}}{V_S}\right)^{1/3}\right] \tag{11}$$

with the constraint that X/D not exceed 0.5.

Early sintering of most metals is dominated by surface diffusion controlled neck growth with little shrinkage, while late in sintering there is no neck growth, but an increase in density and coordination number. As sintering progresses, the local sintering stress decreases while the bulk sintering stress remains nearly constant. Other examples of experimentally measured stress for no sintering shrinkage are given in the literature [33,43,59-63].

The capillary stress reflects the microstructure scale as determined by surface energy and particle size. Thermal softening is necessary to lower the component threshold strength to a level comparable to the sintering stress. With larger particles and lower sintering stresses, more thermal softening is required for densification. When the temperature dependent strength drops to approach the sintering stress, then rapid shrinkage occurs by plastic flow [64-68]. Hence, the key to understanding rapid sintering densification comes from balancing sintering stress and strength.

Sintering Strength

In situ strength arises from the sinter bonds formed between contacting particles as evident by the fractured necks in Fig. 1. The sintered strength depends on the inherent material strength $_o(T)$ at the test temperature (grain size corrected), percent of interface area involved in the bond [28,54], and stress concentration factor associated with the sharp neck radius [47,69-71]. In sintered porous structures, the initial sintering strength varies with the square of the neck size X to particle size D ratio $(X/D)^2$ and coordination number N_C, giving a measured *in situ* sinter bond strength $_S$ analogous to Eq. 10,

$$\sigma_S = \frac{\sigma_o}{\mathrm{K}} V_S \frac{N_C}{\pi}\left(\frac{X}{D}\right)^2 \tag{12}$$

where is the stress concentration factor that reduces the test strength in proportion to the neck curvature. From stress concentration concepts [72], it is inversely proportional to the curvature at the base of the neck, which depends on the neck size ratio (X/D), giving,

$$\mathrm{K} = \frac{1}{2}\left(\frac{D}{X}\right)^2 \tag{13}$$

The maximum neck size ratio X/D is near 0.5, but in cases where the dihedral angle is

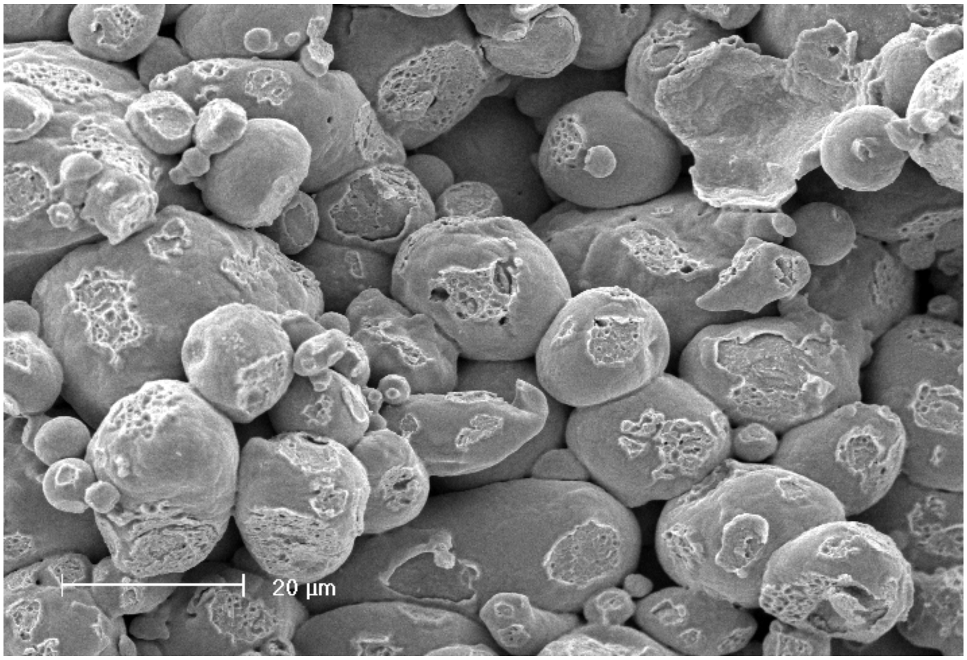

Figure 1. Fracture surface on a sintered bronze structure, showing the ductile tearing of the microstructure at the interparticle necks, indicative that the source of strength is the bond between particles, in agreement with this model.

below 60° the final neck size is limited as follows:

$$\frac{X}{D} = \sin\left(\frac{\phi}{2}\right) \tag{14}$$

Since *X/D* peaks at 0.5, *K* effectively becomes a constant of 2 after the initial stage of sintering.

In solid-state sintering, the dihedral angle links the solid-solid (grain boundary) energy with the solid-vapor surface energy,

$$\gamma_{SS} = 2\gamma_{SV}\cos\left(\frac{\phi}{2}\right) \tag{15}$$

while in liquid phase sintering it links the solid-solid (grain boundary) energy to the solid-liquid surface energy,

$$\gamma_{SS} = 2\gamma_{SL}\cos\left(\frac{\phi}{2}\right) \tag{16}$$

Thus, if not limited by the dihedral angle, then the peak neck size ratio (*X/D*) is near 0.5. If the dihedral angle is under 60°, then the peak sintered density and strength are limited by the dihedral constraint in Eq. 14. Densification induces new grain contacts leading to further strengthening, since the coordination number is linked to the density by Eq. 9.

Transverse rupture strength tests during sintering provide a basis for comparison of the sintering strength with the expectations from Eq. 12. The transverse rupture tests give approximately 1.6 to 2.1 times higher strength when compared to the tensile strength [1]. Alternatively, the stress concentration factor provides an equal, but opposite, compensation when *X/D* reaches 0.5. As an example of the strength attained during sintering, Lal [34] measured 22 m loose spherical bronze powder for *in situ* strength after heating to 75% density at 850°C.

Using thermal softening data from Shoales and German [24], the calculated bulk *in situ* strength using Eq. 12 is 37 MPa while the measured *in situ* transverse strength is 32 MPa. Similarly, using data from Shoales [23] for compacted 26 m bronze, gives a predicted strength at 800°C of 46 MPa which compares favorably with a measured value at 48 MPa.

Most metals have surface energies between 1 and 2 J/m^2. Consequently, significant changes in the sintering stress needed to induce rapid densification is via small particles. For example, 10 m stainless steel powder used in injection molding has a local sintering stress near 6 MPa after 2% shrinkage (corresponding to a bulk stress near 0.7 MPa). As neck growth and densification progress, this stress falls. At 96% density the local and bulk sintering stresses are both about 3.5 MPa. For a large powder, the sintering stress can be as small as 0.02 MPa. These are not high stresses, so most large metal powders sinter bond (strengthen) but do not sinter densify because in Eq. 2 is negative or near zero. Large powders are sufficiently strong when compared to the sintering stress that they resist densification during sintering. For 0.05 m nickel powder which showed densification by 300°C, the calculated local sintering stress $_L$ is over 1000 MPa while the parent material strength is 140 MPa [73]. On a bulk scale, at 300°C the sintering stress is 80 MPa (Eq. 10) and the strength is 16 MPa (Eq. 12). Since the sintering stress is above the *in situ* strength, the 0.05 m Ni powder started densification at a low temperature. As the particle size increases, the lower sintering stress requires a progressively higher temperature before densification is evident. Thus, small particles sinter densify because of a high inherent sintering stress as compared with the *in situ* strength.

Atomic Motion

Besides net sintering stress, atomic mobility influences densification. Sintering will not occur without thermally induced atomic motion, as evident by the lack of sintering in most powders at room temperature. Neck size depends on the cumulative amount of atomic motion over time. Surface transport mechanisms (evaporation-condensation and surface diffusion) move atoms on the pore surfaces, giving particle bonding and compact strengthening, but do not produce densification. Surface diffusion dominates the low temperature sintering of most metals. Bulk transport processes (volume diffusion, grain boundary diffusion, plastic flow, dislocation climb) simultaneously promote neck growth and shrinkage by moving mass from between particles to the interparticle bond. Diffusion processes give slow densification. Plastic flow is active when the microstructure is highly curved, but dislocation generation at the interparticle bonds decays during sintering [68,74,75]. High temperature plastic flow correlates with sintering densification and higher stresses give higher shrinkage rates [76,77]. Viscous flow densification occurs in metals with liquid phases on the grain boundaries [36]. Consequently, it is possible to model all forms of sintering with viscous flow concepts using a Bingham model for densification. Sintering by diffusion processes is slow. On the other hand, for fast sintering of large particles, as desired by industry, rapid densification by viscous or plastic flow is more attractive.

An opportunity for sintering densification is apparent when grain boundary wetting liquids form in the microstructure. Mass transport is very rapid in the presence of a liquid phase, often over 100-times faster than in solids. However, formation of a liquid is not sufficient to ensure densification since the solid phase must be soluble in the liquid to generate significant atomic flux [3,28,78,79]. It is the combined solubility and atomic mobility that determines the sintering rate. Liquids with no solubility for the solid give no densification benefit beyond that from solid-state sintering of the skeleton [80]. In large particle systems, such as the popular copper bonded steels [1], copper induces interparticle sinter bonding and compact strengthening, but not densification. Consequently, net sintering dimensional change for a 100 μm particle size system is nearly zero at the typical 1120°C sintering temperature.

Thermal Softening

An opportunity for sintering densification of large powders in short sintering times comes through analysis of the material strength evolution during sintering. Wrought materials weaken at high temperatures, a feature known as thermal softening. For example, at a strain rate of 10^{-4} 1/s the yield strength of copper drops 31-fold between room temperature and 1000°C and low alloy steel loses 60% of its room temperature strength by 600°C [73,81]. If thermal softening is countered by dispersoids or strengthening inclusions, then the sintering densification rate also decreases [32,82-88].

Relatively little strength data are taken in the range of temperatures where sintering occurs. Analysis of 316L stainless steel strength versus test temperature shows zero strength at the melting temperature [89]. Normally tensile properties are measured at non-constant strain rates ranging from 10^{-1} to 10^{-5} 1/s. On the other hand, rapid sintering densification generally peaks at strain rates of 10^{-3} 1/s. In the strain rate regions typical to sintering, temperature dominates the measured strength. Copper at 800°C and 10^{-3} 1/s decreases strength by 25% if the strain rate drops by an order of magnitude (strain rate softening), but if temperature goes up 100°C strength falls by 70% (thermal softening). Since temperature effects dominate strength, and tensile strain rates approximate the sintering strain rates during periods of rapid densification where plastic flow is anticipated, nominal tensile properties are reasonable approximations for this sintering model. Indeed, earlier calculations show that the time to propagate heat through the compact is the major limitation in sintering densification rates [90]. Assume slow strain rate, high temperature strength tests provide a information relevant to the sintering stress.

The estimated 1250°C strength for 316L stainless steel is 25 MPa, which is more than the sintering stress for 10 μm injection molding grade powders after just 1% shrinkage. Above 1300°C, the strength falls below 10 MPa, allowing 2% shrinkage before the bulk sintering stress equals the strength. By 1330°C the strength is down to 5 MPa and the sintering stress and *in situ* strength are equal at 72% density, and at 1360°C this balance increases to 94% density. Consequently, injection molding grade stainless steel powder is predicted to rapidly sinter densify at temperatures near 1360°C, in agreement with practice [91]. Substantiation of this prediction comes from an injection molded 316L stainless steel powder (nominal size of 15 μm) [92] using density to calculate sintering stress equals the *in situ* strength. Some injection molded stainless steel is sintered to full density in large 1 m^3 furnaces (with considerable thermal inertia) using hold times of just 40 minutes [93]. Most of this isothermal hold is associated with achieving uniform temperature. Rapid densification occurs with temperatures over 1300°C, as predicted here.

Hence, the difficulty in sintering large particles to full density comes from the combination of a low sintering stress and high *in situ* strength. A pressed compact starts with a green strength between 2 and 20 MPa. Unlike a bulk material that thermally softens, sinter bonding increases the compact strength during heating. Details of the *in situ* strength evolution and thermal softening during sintering were measured in recent research [23,24]. From a green strength of 10 MPa, annealing occurs up to 400°C, lowering the *in situ* strength to 4 MPa. Beyond 400°C the strength climbs rapidly due to sinter bond growth, and peaks at 600°C. Thermal softening dominates the *in situ* strength over 600°C. Sintering gives a progressive strength gain at higher temperatures, but softening is evident from strength measurements taken during cooling from a peak sintering temperature of 800°C. Substantial strengthening occurs on cooling, with a final room temperature strength of almost 700 MPa, although the *in situ* strength at 800°C was 50 MPa. This large strength increase on cooling reflects thermal softening from 800°C.

Although the compacts thermally soften at the higher temperatures, the strength remains high up to nearly the solidus temperature. For these same compacts, parallel dilatometer and differential thermal analysis tests show first melt formation at 861°C. Dilatometer measured *in situ* dimensional change showed no densification up to 600°C, and significant densification over 800°C where the *in situ* strength approaches the calculated sintering stress.

Mechanical View of Sintering Densification

The new view of sintering densification comes from comparison of the compact strength with the sintering stress. The focus shifts from the classic concern over atomic motion to consideration of the mechanical response of the compact. Densification critically depends on the sintering stress exceeding the threshold strength. As temperature increases, the strength and elastic modulus fall and the ductility usually increases, but decreases at high temperatures. Densification by plastic flow is expected when thermal softening lowers the flow stress to a level comparable to the sintering stress. The larger the sintering stress (smaller the particle size), the lower the temperature for the onset of densification during heating. At high temperatures, slow solid-state densification occurs by diffusional creep, while strengthening from bond growth can occur without densification. Accordingly, a notion for full density sintering in short times emerges based on the *in situ* stress. For larger particle sizes with low sintering stresses, sintering densification is hindered by the inherent compact strength. If the compact is thermally softened to a level approaching the sintering stress, then it rapidly densifies. Unfortunately, because of the low sintering stress, more thermal softening is required for large particles that otherwise resist densification. Supporting this concept is recognition that most sintering occurs during heating to the sintering temperature. Accordingly, isothermal holds are very short in industrial sintering. Indeed, most dilatometer traces show more shrinkage during heating than once isothermal conditions are attained, in line with a dominant role from thermal softening as compared with diffusion controlled-densification.

The pathway shown for bronze, where strength increases before densification, has been verified for several materials. For example, mixed 125 μm water atomized iron and copper powders with graphite (2 wt.% Cu and 0.8% C), compacted to 7.37 g/cm^3 has a green strength of 12.1 MPa. After heating at 10°C/min the *in situ* transverse rupture strength increases to 56 MPa at 1100°C, and on cooling to room temperature is over 1000 MPa. The predicted strength at 1100°C is near 44 MPa, while the calculated sintering stress is 3.5 MPa. Since the strength is more than 10-fold higher than the sintering stress, the compact resists sintering densification and only slow creep densification occurs in sintering (less than 0.1% shrinkage). A diffusion-based computer simulation [94] suggests a final density of 7.5 g/cm^3 (0.6% shrinkage) is possible after 120 h at 1120°C. Alternatively, higher temperatures can give sufficient thermal softening for rapid densification. Thus, a fundamental problem in sintering large powders to full density in short sintering times is the *in situ* strength. As particle size increases, the sintering stress decreases, yet surface transport controlled sinter bonding increases the strength at temperature.

Conclusions

Basic stress-strength mechanical ideas are applied to sintering. Unlike bulk materials that thermally soften with heating, the pathway for powder compacts is more complicated. A combination of sinter bonding and thermal softening determines the resistance to densification for both large and small powders. Small powders have higher sintering stresses and prove easier to densify in short times when the *in situ* strength and viscosity fall at high temperatures. On the other hand, large powders have lower sintering stresses such that the *in situ* strength resists densification during sintering. Slow diffusional processes give some densification, but not in time frames compatible with many industrial sintering cycles.

Liquid phases provide a means to lower *in situ* strength during sintering. A low dihedral angle is preferred, but if the dihedral angle approaches zero and the pores are saturated with liquid, then all strength is lost and the component distorts. Since liquid wetting and the solid:liquid ratio depend on temperature, good temperature control is required in these processes. With large powders the sintering stress is low, so only a low *in situ* strength will allow densification. A large change in solid solubility on melt formation is a predictor of sintering densification. From these principles, several alloys can be designed for full density processing in thermal cycles compatible with traditional furnaces.

Acknowledgments

This paper resulted from funding provided by the National Aeronautics and Space Administration (Gravitational Effects on Distortion in Sintering, NAG8-1452, Mike Purvey project manager and Witold Palosz project scientist) and the National Science Foundation (Protocol Development for Net Shape Powder Metal Part Production, DMI 02-00554, Delcie Durham and K. L. Murty as co-program managers).

References

1. R. M. German: *Powder Metallurgy of Iron and Steel*, Wiley, New York, NY, 1998.
2. G. C. Kuczynski: *Trans. TMS-AIME.* **185** (1949) 169-178.
3. R. M. German: *Sintering Theory and Practice*, Wiley, New York, NY, 1996.
4. W. Schatt: *Sci. Sinter.* **25** (1993) 99-107.
5. C. S. Morgan, C. J. Mchargue, and C. S. Yust: *British Ceramic Soc. Proc*. **No. 3** (1965) 177-184.
6. M. H. Tikkanen, and S. Ylasaari: *Modern Developments in Powder Metallurgy*, vol. 1, H. H. Hausner (ed.), Plenum Press, New York, NY, 1966, pp. 297-309.
7. G. H. Gessinger, F. V. Lenel, and G. S. Ansell: *Trans. ASM.* **61** (1968) 598-604.
8. G. H. Gessinger: *Z. Metallkde*. **66** (1969) 238-243.
9. C. S. Morgan: *Modern Developments in Powder Metallurgy*, vol. 4, H. H. Hausner (ed.), Plenum Press, New York, NY, 1971, pp. 231-240.
10. E. Navara, and K. E. Easterling: *Inter. J. Powder* Met. **7** (4) (1971) 11-16.
11. C. S. Morgan: *High Temp.-High Press*. **3** (1971) 317-324.
12. F. V. Lenel, G. S. Ansell, and R. C. Morris: *Modern Developments in Powder Metallurgy,* vol. 4, H. H. Hausner (ed.), Plenum Press, New York, NY, 1971, pp. 199-220.
13. D. L. Yenawine, and W. R. Upthegrove: *Metall. Trans.* **3** (1972) 3035-3036.
14. C. S. Morgan: *Phys. Sintering*. **5** (1973) 31-40.
15. J. E. Sheehan, F. V. Lenel, and G. S. Ansell: *Sintering and Related Phenomena*, G. C. Kuczynski (ed.), Plenum Press, New York, NY, 1973, pp. 201-208.
16. J. E. Sheehan, F. V. Lenel, and G. S. Ansell: *Scripta Met*. **7**, (1973) 809-814.
17. E. Friedrich, and W. Schatt: *Powder Met.* **23** (1980) 193-197.
18. L. I. Tuchinskii: *Soviet Powder Met. Metal Ceram*. **21** (1982) 849-853.
19. W. A. Kaysser, M. Amtenbrink, and G. Petzow: *Sintering - Theory and Practice*, D. Kolar, S. Pejovnik and M. M. Ristic (eds.), Elsevier Scientific, Amsterdam, Netherlands, 1982, pp. 275-282.
20. W. Schatt, and K. P. Wieters: *Powder Met. Inter*. **18** (1986) 135-139.

21. S. V. Raman, R. H. Doremus, and R. M. German: *J. Physique.* **47** (1986) 225-230.
22. R. A. Andrievski: *Inter. J. Powder Met.* **30** (1994) 59-66.
23. G. A. Shoales, and R. M. German: *Metall. Mater. Trans.* **29A** (1998) 1257-1263.
24. G. A. Shoales, and R. M. German: *Metall. Mater. Trans.* **30A** (1999) 465-470.
25. E. A. Olevsky: *Mater. Sci. Eng.* **R23** (1998) 41-100.
26. J. K. Mackenzie, and R. Shuttleworth: *Proc. Phys. Soc.* **62** (1949) 833-852.
27. R. L. Coble: *J. Amer. Ceramic Soc.* **41** (1958) 55-62.
28. R. Raj, and C. K. Chyung: *Acta Met.* **29** (1981) 159-166.
29. R. F. Cooper, D. L. Kohlstedt, and K. Chyung: *Acta Met.* **37** (1989) 1759-1771.
30. W. J. Kim, and D. W. Kum: *Mater. Trans. Japan Inst. Met.* **40** (1999) 760-764.
31. W. E. Luecke, and S. M. Wiederhorn: *J. Amer. Ceramic Soc.* **82** (1999) 2769-2778.
32. C. H. Hsueh, A. G. Evans, R. M. Cannon, and R. J. Brook: *Acta Met.* **34** (1986) 927-936.
33. P. Z. Cai, G. L. Messing, and D. L. Green: *J. Amer. Ceramic Soc.* **80** (1997) 445-452.
34. A. Lal: *Mechanisms and Mechanics of Shape Loss During Supersolidus Liquid Phase Sintering*, Ph. D. Thesis, Engineering Science and Mechanics Department, The Pennsylvania State University, University Park, PA, 1999.
35. J. Canel, and D. Bouvard: *Advances in Powder Metallurgy and Particulate Materials - 1996*, Metal Powder Industries Federation, Princeton, NJ, 1996, pp. 7.47-7.55.
36. R. M. German: *Metall. Mater. Trans.* **28A** (1997) 1553-1567.
37. R. Ganesan, A. Griffo, and R. M. German: *Metall. Mater. Trans.* **29A** (1998) 659-664.
38. A. Upadhyaya, R. G. Iacocca, and R. M. German: *J. Met.* **51 (4)** (1999) 37-40.
39. Y. Liu, J. Liu, and R. M. German: *Advances in Powder Metallurgy and Particulate Materials*, vol. 1, Metal Powder Industries Federation, Princeton, NJ, 1999, pp. 3.177-3.188.
40. A. Tewari, A. M Gokhale, and R. M. German: *Acta Mater.* **47** (1999) 3721-3734.
41. N. Pashias, D. V. Boger, J. Summers, and D. J. Glenister: *J. Rheol.* **40** (1996) 1179-1189.
42. A. Upadhyaya: *A Microstructure-Based Model for Shape Distortion During Liquid Phase Sintering*, Ph. D. Thesis, Department of Engineering Science and Mechanics, The Pennsylvania State University, University Park, PA, 1998.
43. R. A. Gregg, and F. N. Rhines: *Metall. Trans.* **4** (1973) 1365-1374.
44. E. H. Aigeltinger: *Inter. J. Powder Met. Powder Tech.* **11** (1975) 195-203.
45. K. S. Hwang, R. M. German, and F. V. Lenel: *Metall. Trans.* **18A** (1987) 11-17.
46. L. C. De Jonghe, and M. L. Rahaman: *J. Amer. Ceramic Soc.* **67** (1984) C214-C215.
47. L. U. J. T. Ogbuji: *Sci. Sintering.* **18** (1986) 21-31.
48. R. Raj: *J. Amer. Ceramic Soc.* **70** (1987) C210-C211.
49. S. T. Lin, and R. M. German: *J. Amer. Ceramic Soc.* **71** (1988) C432-C433.
50. J. Svoboda, H. Riedel, and H. Zipse: *Acta Met. Mater.* **42** (1994) 435-443.
51. A. S. Helle, K. E. Easterling, and M. F. Ashby: *Acta Met.* **33** (1985) 2163-2174.
52. A. J. Markworth: *Scripta Met.* **6** (1972) 957-960.
53. W. M. Goldberger: data presented at the 1999 Advanced Technology Program, National Institute of Standards and Technology, San Jose, California, 17 November 1999.
54. A. C. Nyce, and W. M. Shafer: *Inter. J. Powder Met.* **8** (1972) 171-180.
55. M. C. Dang, J. J. Blandin, and B. Baudelet: *Acta Mater.* **44** (1996) 3991-4002.
56. A. K. Dahle, and L. Arnberg: *Acta Mater.* **45** (1997) 547-559.
57. H. F. Fischmeister, E. Arzt, and L. R. Olsson: *Powder Met.* **21** (1978) 179-187.
58. Z. Z. Du, and A. C. F. Cocks: *Acta Met. Mater.* **40** (1992) 1981-1994.
59. K. R. Venkatachari, and R. Raj: *J. Amer. Ceramic Soc.* **69** (1986) 499-506.
60. M. N. Rahaman, L. C. De Jonghe, and R. J. Brook: *J. Amer. Ceramic Soc.* **69** (1986) 53-58.
61. T. Cheng, and R. Raj: *J. Amer. Ceramic Soc*. **71** (1988) 276-280.
62. V. C. Ducamp, and R. Raj: *J. Amer. Ceramic Soc.* **72** (1989) 798-804.
63. J. Besson, and M. Abouaf: *J. Amer. Ceramic Soc.* **75** (1992) 2165-2172.
64. W. Schatt, and J. I. Boiko: Sci. Sintering. **24** (1992) 95-103.
65. W. Schatt, W. Hermel, E. Friedrich, and P. Lanyi: *Sci. Sintering.* **15** (1983) 5-26.
66. E. Friedrich, and W. Schatt: *Sci. Sintering.* **15** (1983) 63-71.
67. W. Schatt, and E. Friedrich: *Sci. Sintering.* **16** (1984) 63-72.
68. W. Schatt, E. Friedrich, and K. P. Wieters: *Rev. Powder Met. Phys. Ceram.* **3** (1986) 1-111.

69. X. Xu: *Densification, Microstructure, and Strength Evolution During Sintering,* Ph. D. Thesis, Department of Engineering Science and Mechanics, The Pennsylvania State University, University Park, PA, 2000.
70. K. E. Easterling, and A. R. Tholen: *Modern Developments in Powder Metallurgy*, vol. 4, H. H. Hausner (ed.), Plenum Press, New York, NY, 1971, pp. 221-230.
71. Y. I. Boiko, Y. A. Geguzin, and Y. I. Klinchuk: *Soviet Powder Met. Metal Cer.* **21** (1982) 181-183.
72. R. C. Hibbeler: *Mechanics of Materials*, second edition, Prentice-Hall, Englewood Cliffs, NJ, 1994, pp. 157-166.
73. E. A. Brandes, and G. B. Brook: *Smithells Metals Reference Book*, seventh edition, Butterworh Heinemann, Oxford, UK, 1992, p. 22.74.
74. W. Schatt, H. E. Exner, E. Friedrich, and G. Petzow: *Acta Metall.* **30** (1982) 1367-1375.
75. K. E. Easterling: *Inter. J. Powder Met.* **7 (2)** (1971) 29-37.
76. K. E. Easterling: *Phys. Sintering*, **4** (1972) 75-87
77. W. Schatt, and E. Friedrich: *Powder Met.* **28** (1985) 140-144.
78. R. M. German, and B. H. Rabin: *Powder Met.* **28** (1985) 7-12.
79. D. S. Madan, and R. M. German: *Powder Met.* **33 (1)** (1990) 45-52.
80. J. L. Johnson, and R. M. German: *Metall. Mater. Trans.* **27B** (1996) 901-909.
81. P. Han (ed.): *Tensile Testing*, ASM International, Materials Park, OH, 1992, pp. 95-96.
82. N. M. Rahaman, and L. C. De Jonghe: *J. Mater. Sci.* **22** (1987) 4326-4330.
83. M. W. Weiser, and L. C. De Jonghe: *J. Amer. Ceramic Soc.* **71** (1988) C125-C127.
84. C. H. Hsueh: *J. Amer. Ceramic Soc.* **71** (1988) C314-C315.
85. A. R. Boccaccini: *Sci. Sintering.* **23** (1991) 151-161.
86. S. J. Kiss, and E. Kostic: *Powder Met. Inter.* **24** (1992) 247-250.
87. O. Sudre, G. Bao, B. Fan, F. F. Lange, and A. G. Evans: *J. Amer. Ceramic Soc.* **75** (1992) 525-532
88. Y. Nakada, and T. Kimura: *J. Amer. Ceramic Soc.* **80** (1997) 401-406.
89. J. R. Davis (ed.): *Stainless Steels*, ASM International, Materials Park, OH, 1994, pp. 505-524.
90. A. Belhadjhamida, and R. M. German: *Advances in Powder Metallurgy and Particulate Materials - 1993*, vol. 3, Metal Powder Industries Federation, Princeton, NJ, 1993, pp. 85-98.
91. R. M. German, and A. Bose: *Injection Molding of Metals and Ceramics*, Metal Powder Industries Federation, Princeton, NJ, 1997, pp. 259-260.
92. R. M. German: *Powder Metallurgy Science*, second edition, Metal Powder Industries Federation, Princeton, NJ, 1994, p. 292.
93. K. L. Lim: personal communication, Advanced Materials Technologies, Singapore.
94. F. B. Swinkels, and M. F. Ashby: *Acta Met.* **29** (1981) 259-281.